Removal of fluoride from spiked water in the batch or static mode and also in the column or dynamic mode

Arunima Sarma[a,*], Krishna G. Bhattacharyya[b]

[a]Department of Chemistry, Morigaon College, Morigaon 782105, Assam, India, Tel. +91 9435147228;
email: arunimsarma0906@gmail.com
[b]Department of Chemistry, Gauhati University, Guwahati 781014, Assam, India, Tel. +91 9864031987;
email: kgbhattacharyya@gmail.com

ABSTRACT

Mature leaves of the neem tree (*Azadirachta indica*) were converted into fine powder, the neem leaf powder (NLP), which was used for adsorption of fluoride from water. Adsorption was 82.6% at pH 2.1, 97.5% at pH 7.0 and 99.4% at pH 10.0 at a fluoride concentration of 15 mg/L. Adsorption kinetics conformed to pseudo-second-order model with a rate coefficient of 2.04×10^{-2}–11.83×10^{-2} min/mg/g for a NLP amount of 1.0–6.0 g/L. The adsorption enthalpy, ΔH, decreased slightly from 26.06 to 24.85 kJ/mol as the fluoride concentration increased (2.50–20 mg/L). In the same concentration range, the adsorption entropy, ΔS, varied from −66.92 to 86.47 J/mol/K. Spontaneity was ensured by Gibbs energy decrease from −5.75 to −0.99 kJ/mol (fluoride 15.0 mg/L) and from −1.79 to −2.65 kJ/mol (fluoride 20.0 mg/L) in the temperature range of 308–318 K. However, at lower concentrations of fluoride, ΔG had values >0 which still decreased with increasing temperature. The influence of competing ions on fluoride adsorption by NLP showed a significant influence of Cl^-, HCO_3^-, SO_4^{2-}, NO_3^- and HPO_4^- ions. Dynamic study on a NLP column showed a breakthrough volume of 2,800 mL for a fluoride loading of 20 mg/L, a flow rate of 0.4 mL/min and a column bed depth of 1.5 cm.

Keywords: Fluoride removal; Neem leaf powder; Column adsorption; Water treatment

1. Introduction

Water with a high fluoride content is found mostly in calcium-deficient ground waters in many basement aquifers, such as granite and gneiss, in geothermal waters and in some sedimentary basins. According to the World Health Organization [1], fluoride can be present in drinking water and it is considered beneficial at levels about 0.7 mg/L but hazardous if it exceeds 1.5 mg/L. Groundwater with a high fluoride concen-tration occurs in many areas of the world including large parts of Africa, China, the Middle East and southern Asia (India, Sri Lanka). In India, 25 million people in 19 states and union territories are affected by fluoride and another 66 million are thought to be at risk including six million children below the age of 14 years [2]. Fluoride levels in groundwater in India are from below 0.5 mg/L to as high as 35 mg/L [3]. Nearly 100,000 villagers in the remote Karbi Ang-long district in the north-eastern state of Assam are affected by excessive fluoride levels in groundwater

*Corresponding author.

and many have been crippled for life by severe anaemia, stiff joints, painful and restricted movement, mottled teeth and kidney failure. Taking the serious health effects into consideration, several technologies, including precipitation–coagulation, adsorption, ion exchange, membrane separation and electrodialysis, have been developed for fluoride removal [4]. Among these methods, adsorption is considered as an effective, environment-friendly and economical method for removing excessive fluoride from drinking water because adsorption is a highly effective, direct, simple and relatively low-cost method.

Adsorption has been reported as one of the most effective methods for fluoride removal [4]. Activated carbon, natural minerals, fish bone charcoal, coconut shell carbon and rice husk carbon are some of the materials that have shown different degrees of success in fluoride adsorption [5]. Recently, considerable interest has been generated in the application of biosorbent materials based on animal or plant biomass for the removal of pollutants [5,6]. These materials bind ions onto their surface through interactions of the ions with surface functional groups. This methodology has the important advantages of low operating cost, minimum chemical and biological sludge, high efficiency in dilute solutions, no requirement of nutrient supplement, etc. The biomaterials have been shown to be as effective as commercial adsorbents with respect to cost-effectiveness in industrial wastewater treatment, and the materials prepared from microbial as well as plant sources have received considerable attention [7,8].

One recent trend in the use of biomass for pollution abatement is the use of waste tree leaves to prepare adsorbent materials [9,10]. In the present work, an adsorbent material was prepared from mature neem (*Azadirachta indica*) leaves for use in the removal of fluoride from spiked water.

2. Experimental section

2.1. Materials

Mature neem leaves were procured from neem (*A. indica*) trees in and around Morigaon, India. The leaves were washed with water several times to remove accumulated dust and soluble impurities, dried first in the Sun and then in an air oven at 333–343 K for several hours till the leaves became crisp. These were crushed into fine powder and washed again with distilled water to remove soluble plant pigments till the filtrate was colourless. The powder was dried at 380 K, sieved and the fractions of particle size, 74–149 μm, were preserved as the adsorbent, neem leaf powder (NLP).

A stock solution of concentration 100 mg/L with respect to fluoride was prepared by dissolving 221 mg of anhydrous sodium fluoride in double-distilled water and diluting the same to 1,000 mL [11]. The stock solution was appropriately diluted to get the test solutions of desired fluoride concentration. The pH of the aqueous fluoride solution was 6.7.

2.2. Adsorption process

Stoppered plastic bottles of 100-mL capacity were used for adsorption experiments. A fixed amount of the adsorbent, NLP, was mixed with 50 ml of fluoride solution of desired concentration and the mixture was agitated for a predetermined time interval using a water bath incubator shaker (Model Q5247, Navayug, India). Fluoride remaining unadsorbed was determined with a UV–vis spectrophotometer (Beckman Coulter DU Series 700) following the SPADNS reagent method at $\lambda_{max} = 570$ nm [11]. The mixed SPADNS reagent used in this method was prepared by mixing equal volumes of SPADNS solution and zirconium oxychloride solution.

All the studies were performed at a constant temperature of 303 K, representing the ambient environmental conditions.

2.3. Fixed bed column adsorption

For treating wastewater in large quantities, a fixed-bed reactor is often more preferable to a batch reactor. To design a fixed-bed adsorption process, it is important to know the adsorption capacities of the materials and the kinetics of adsorbate–adsorbent interactions. The batch adsorption studies conducted in this work provide important information to carry out dynamic adsorption using the same set of materials as adsorbents in the fixed-bed system and fluoride as the adsorbate. However, in case of biosorbents, the low mechanical and chemical resistance including difficulty in solid/liquid separation restricts their application in continuous flow experiments. These drawbacks can be overcome by converting the biosorbent into granular form, if necessary, using a suitable binder.

In the present work, the powdered biosorbent was converted to granular form using locally available clay used for making earthenware as the binder and the column experiments were performed to find out the various column parameters. The conversion of the biosorbent into granular form was done by preparing slurry of local clay and NLP in the weight ratio of 1:1 in the minimum amount of distilled water. The slurry was introduced into a handmade cone and extruded

into small pieces (1.0-mm diameter) by applying pressure manually. The pieces were cut into 1–3-mm pieces. These were cured by putting them inside an air oven at 393 K for 6 h. The dry granules were kept in a desiccator.

The fixed-bed adsorption was carried out in a glass column of 30.0-cm length and 3.0-cm internal diameter. The column bed was prepared by dry-packing technique by inserting the required amount of the adsorbent between two glass wool plugs to prevent absorbent bleeding. The bed was rinsed with distilled water and left overnight to ensure a closely packed arrangement of particles without voids, channels or cracks.

The column was fed continuously with aqueous NaF solution of particular concentration at a desired volume flow rate. The flow rate was maintained constant during the experiments by keeping constant the influent level in the column with a reservoir of influent solution (NaF) above the column. The bed height, the rate of flow and the concentration of the solute could be varied and the column adsorption was monitored by continuously measuring the concentration of fluoride in the effluent with time or volume flowing out of the column. The flow through the column was continued till the outlet and inlet concentrations were equal. The breakthrough curves were obtained by plotting C_v/C_o against the cumulative volume of the fluoride solution passing through the column, where C_o and C_v were the inlet and outlet concentrations of fluoride, respectively. The effluent samples were collected at a predetermined volume interval of 25 mL in 50-mL plastic bottles and analysed for the remaining fluoride concentration by the SPADNS method.

3. Results and discussion

3.1. Adsorbent characterization

The NLP had a slightly acidic reaction with water yielding a pH of 5.6 for 10% slurry. Methylene blue adsorption and application of Langmuir isotherm yielded a specific surface area of 21.45 m^2/g for the adsorbent powder. Scanning electron micrographs of the powder, reported earlier, showed particles of various sizes and shapes that had nonuniform surface topography [9]. The particles had broken edges with steps and kinks visible in the micro scale. FTIR spectra of the powder, also reported earlier [9], showed the presence of a variety of functional groups, such as –OH, –NH$_2$, >C=N–, ≡C–C≡, ≡C–N<, ≡C–O–, >C=O, >C=C< and >C=S, on the surface of the particles. The interaction properties of the NLP particles are likely to be determined by these groups. The NLP showed

considerable presence of Ca, Cu, Fe, K and Mn as observed from XRF measurements [9].

3.2. Adsorption efficiency at different pH

The pH of the medium had a significant influence on the uptake of fluoride by NLP (Fig. 1). Thus, at a fluoride concentration of 15 mg/L and a NLP amount of 1 g/L, the adsorption was 82.6% at pH 2.1, 97.5% at pH 7.0 and 99.4% at pH 10.0. Since adsorption was very high near neutral conditions, all subsequent experiments were carried out without adjusting the pH of the fluoride solution. The extents of adsorption varied with a change in the fluoride concentration.

In most of the solid/liquid adsorption processes, the solution pH has a major influence on the adsorption capacity of the adsorbent due to the competition for the active sites by hydroxyl ions. However, in this work, there is a wide range of pH (5–10) over which fluoride removal is considerable. This is much better compared to any prior report on the effects of pH on fluoride adsorption. For example, Zhang et al. have recently reported that the fluoride removal efficiencies could reach up to 86.2, 83.2 and 76.5% at pH 11 at initial fluoride concentrations of 10, 20 and 30 mg/L, respectively [4]. Mohapatra et al. have shown that the fluoride removal efficiency of Mg-doped nano-Fe$_2$O$_3$ was only ~30% at pH 11 and at an initial fluoride concentration of 10 mg/L [12]. Swain et al. have reported a fluoride removal efficiency of ~38% at pH 11 for alginate-entrapped Fe(III)–Zr(IV) binary mixed oxide [13].

The considerably low adsorption (33.67%) at pH 2.0 at a fluoride concentration of 2.5 mg/L was attributed to the surface layer of H$_3$O$^+$ ions providing few bare sites for interaction with sparingly distributed fluoride ions [14]. As the pH was increased, some of
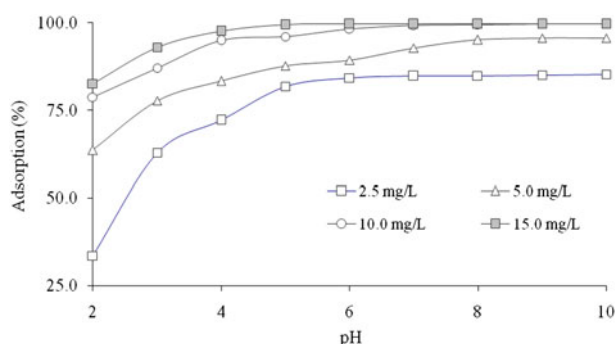
Fig. 1. Effects of pH on adsorption of fluoride on NLP (Fluoride: 2.5, 5.0, 10.0, 15.0 mg/L, NLP: 1.0 g/L, temperature: 303 K).

the H_3O^+ ions left the NLP surface making those sites available for specific fluoride ion adsorption. Some of the fluoride ions might also be held through anion exchange with surface functional groups such as amino, carboxyl and thiol at acidic pH [15]. These anions are also likely to be protonated at acidic pH and the fluoride ions may be held by them. Relative inhibition of adsorption at basic pH could be attributed to the increase in hydroxyl ion concentration that promotes formation of aqua complexes with fluoride, thereby decreasing adsorption [16]. However, the fluoride adsorption efficiency at pH 6.5–7.0 was very high and significant for scaling up the technology for contaminated water treatment.

3.3. Influence of fluoride concentration and NLP loading

The effect of initial concentration of fluoride (2.5–20 mg/L) on adsorption capacity q (mg/g) of NLP was studied without adjustment of the pH using an interaction time of 60 min at different NLP loadings of 1.0–6.0 g/L. Fig. 2 shows that the amount, q, of fluoride removed by unit mass of NLP decreased from 17.8 to 3.0 mg/g for the range of fluoride concentrations with NLP loading changing upward from 1.0 to 6.0 g/L. The removal efficiency was 88.6% at a fluoride concentration of 2.5 mg/L decreasing to 80% at a fluoride concentration of 20 mg/L. At higher fluoride concentrations, the available surface sites on NLP are exhausted and the adsorption capacity decreases.

Tian et al. have reported that the equilibrium adsorption capacity of fluoride on modified native

cellulose fibres (1.0 g/L) showed a rising trend with increasing fluoride concentration (C_o) of 1.5–7.5 mg/g for C_o values of 1.8–12.8 mg/L [17]. Similar results were obtained by Viswanathan and Meenakshi [18] with protonated chitosan beads as the adsorbent for fluoride with q_e varying from 2.18 to 3.37 mg/g for C_o in the range of 11–17 mg/L. The results obtained with NLP are comparable with those of the modified native cellulose adsorbent and are better than the protonated chitosan beads.

3.4. Adsorption kinetics

Adsorption equilibrium was determined by carrying out the experiments at different time intervals with different NLP loadings (1.0–6.0 g/L) and fluoride concentrations (2.5–20 mg/L) at 303 K. The amount adsorbed (q_t) increased up to an interaction time of 80 min after which the adsorption remained constant (Fig. 3). Thus, the time necessary for NLP–fluoride interactions to reach equilibrium could be considered as 80 min. The percentage adsorption also increased with time and at the equilibrium time, about 96–99% of the fluoride was removed from water. The relatively short equilibrium time and high-removal efficiency indicate that NLP has a considerable degree of affinity towards fluoride. The initial rapid adsorption of fluoride (Fig. 3) is due to the participation of specific functional groups and active surface sites [16] in interacting with fluoride ions. A large fraction of fluoride was removed within 10 min of interaction in all
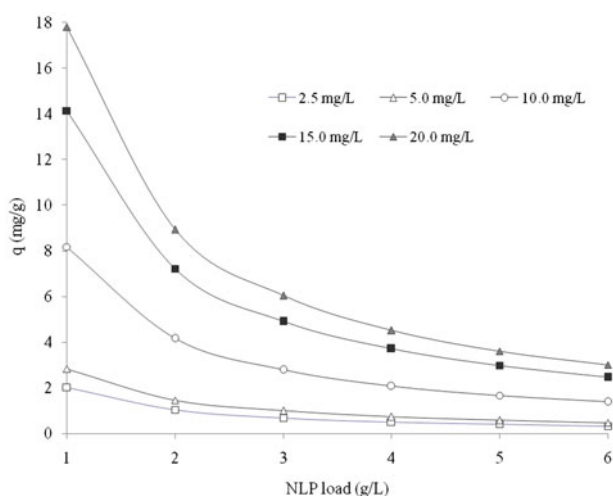
Fig. 2. Variations in the amount adsorbed per unit mass (q mg/g) at different fluoride concentrations (2.5, 5.0, 10.0, 15.0, 20.0 mg/L) and at NLP loadings of 1.0–6.0 g/L (equilibrium time: 60 min, temperature: 303 K).
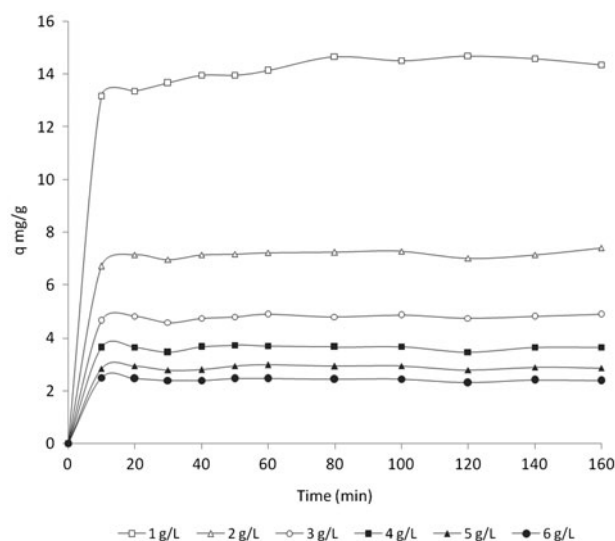
Fig. 3. Amount of fluoride adsorbed per unit mass of NLP at different time intervals (NLP: 1.0–6.0 g/L, fluoride: 20 mg/L, temperature: 303 K).

the experimental variations. Various models were used to work out the kinetic order of the adsorbate–adsorbent interactions [2]. When adsorption is preceded by diffusion through a boundary, the kinetics follows the pseudo-first-order mechanism given by the Lagergren equation:

$$\log(q_e - q_t) = \log\ q_e - (k_1/2.303)\,t \tag{1}$$

In such a case, plots of $\log(q_e - q_t)$ vs. t yielded straight lines, but the values of log (q_e) obtained from the intercepts of the plots did not tally with those obtained experimentally and the first-order Lagergren model was considered as inadequate to explain the kinetics. Application of second-order kinetics using the equation:

$$t/q_t = 1/(k_2 q_e^2) + (1/q_e)\,t \tag{2}$$

$k_2 q_e^2$ is the initial adsorption rate as $t \to 0$ by plotting t/q_t vs. t yielded linear plots (Fig. 4) with better compliance between q_e from the plots and those from the experiments (Table 1). The rate coefficients obtained from the plots are given in Table 1. The second-order rate coefficient had values of 2.04×10^{-2}–11.83×10^{-2} min mg/g for NLP loadings of 1.0–6.0 g/L and the increase was most likely due to an increase in the surface area of the biosorbent NLP, available to fluoride ions. The experimental q_e values varied from 18.29 to 3.10 mg/g and the q_e values from second-order plots varied from 18.87 to 3.18 mg/g with the percentage of variation being 6.7–2.52% (Table 2).
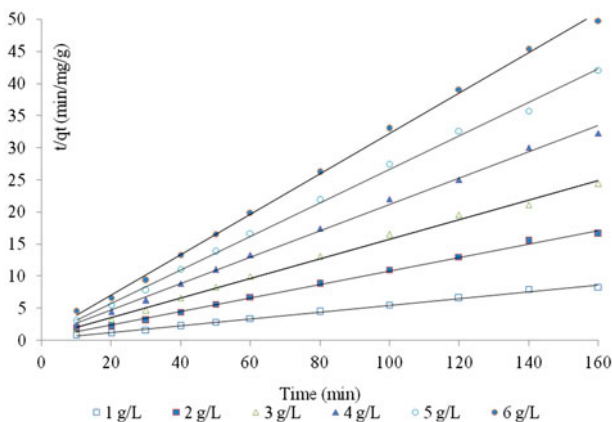
Fig. 4. Second-order kinetic plots for fluoride (20 mg/L) adsorption on NLP (1.0 g/L–6.0 g/L) at a temperature of 303 K.

Thus, the second-order kinetics appears to be the most appropriate mechanism for the NLP–F⁻ interactions.

Weber and Morris [19] have shown that if the rate-limiting step is intraparticle diffusion, a plot of amount adsorbed against the square root of contact time gives a straight line passing through the origin according to the equation:

$$q_t = k_i \cdot t^{0.5} \tag{3}$$

In this case, these plots are linear in parts only and they do not have zero intercepts. Therefore, it is difficult to draw definitive conclusions. The intraparticle diffusion rate coefficient, k_i, computed from the linear parts of the plots had values of 3.31×10^{-2}–0.90×10^{-2} mg/g min$^{-0.5}$ (Table 1). When the two processes of adsorption on external surface and intraparticle diffusion are independent of one another, the plots of q_t vs. $t^{0.5}$ appear as two or more intersecting lines, the first one representing surface adsorption, the second one intraparticle diffusion and so on. Adsorption of ions, in such cases, follows a three-step mechanism consisting of (i) transport of ions from the bulk solution to the film surrounding the adsorbent, (ii) transfer from the film to the adsorbent surface leading to surface adsorption and (iii) diffusion from the surface to the internal sites, followed by binding of the ions on the active sites [20,21]. But such type of similar mechanism might not be in operation for fluoride adsorption on NLP (Fig. 5). It is likely that a batch of fluoride ions first adsorbs on the external surface and then, gradually diffuses into the interior, leaving behind a set of adsorption sites on the surface for a second batch of fluoride ions. The small fluoride ions can easily diffuse into pores.

3.5. Equilibrium adsorption capacity

Freundlich [22] and Langmuir [23] isotherms were utilized to obtain the equilibrium adsorption capacity of NLP for fluoride. The two isotherms had convenient expressions:

$$\text{Freundlich isotherm}: \quad q_e = K_f C_e^{1/n} \tag{4}$$

or its linear form,

$$\log(q_e) = \log K_f + 1/n \log C_e \tag{5}$$

$$\text{Langmuir isotherm}: \quad C_e/q_e = (1/bq_m) + (1/q_m)\,C_e \tag{6}$$

Table 1
First- and second-order kinetic parameters for adsorption of fluoride on different amounts of NLP (fluoride concentration: 20 mg/L, temperature: 303 K)

NLP (g/L)	First-order		Second-order		Intraparticle diffusion		
	k_1 (min^{-1}) × 10^3	R	k_2 (g/mg/min) × 10^2	R	k_i (min^{-1})	Intercept	R
1.0	6.91	0.78	2.05	0.99	0.033	17.69	0.19
2.0	9.21	0.92	2.96	0.99	0.023	8.876	0.25
3.0	11.52	0.90	4.62	0.99	0.016	5.922	0.28
4.0	13.82	0.89	7.78	0.99	0.013	4.424	0.30
5.0	16.12	0.92	11.51	0.99	0.009	3.549	0.28
6.0	18.42	0.83	11.83	0.99	0.008	2.955	0.28

Table 2
Differences between experimental q_e and those obtained from first- and second-order plots for adsorption of fluoride on NLP at 303 K (fluoride concentration: 20 mg/L, temperature: 303 K)

NLP load (g/L)	q_e (expt) (mg/g)	First-order kinetics		Second-order kinetics	
		q_e (plot) (mg/g)	Deviation (%)	q_e (mg/g)	Deviation (%)
1.0	18.29	9.87	46.0	18.87	3.07
2.0	9.22	0.54	94.0	9.62	4.16
3.0	6.14	0.31	95.0	6.58	6.67
4.0	4.61	0.64	86.7	4.83	4.55
5.0	3.68	0.21	94.3	3.85	4.42
6.0	3.10	0.24	92.3	3.18	2.52
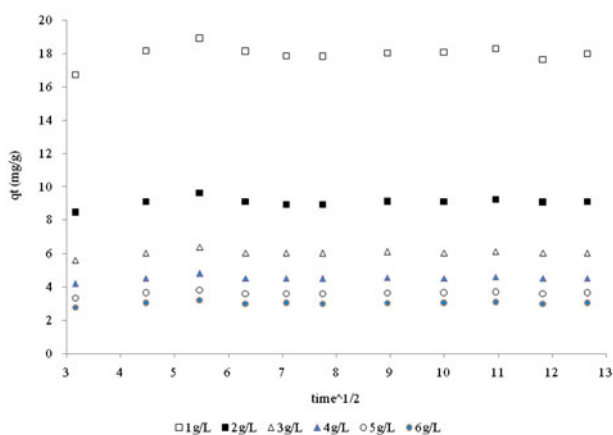
Fig. 5. Plots of Weber–Morris diffusion model for fluoride (20 mg/L) adsorption on NLP (1.0–6.0 g/L) at a temperature of 303 K.

where q_e (mg/g) is the amount of F$^-$ ions adsorbed per gram of NLP at equilibrium, C_e is the concentration (mg/L) of fluoride in the aqueous phase at equilibrium, K_f and $1/n$ (<1) are the Freundlich coefficients and q_m is the Langmuir monolayer capacity (mg/g), i.e. the amount of fluoride required to form a monolayer over the surface of NLP. The adsorption capacities, K_f and q_m, obtained from the slopes and intercepts of the plots (Figs. 6 and 7) are strictly valid when all the adsorption sites have equal affinity for fluoride ions and there is no transmigration of fluoride in the plane of the surface. Sorption data of fluoride
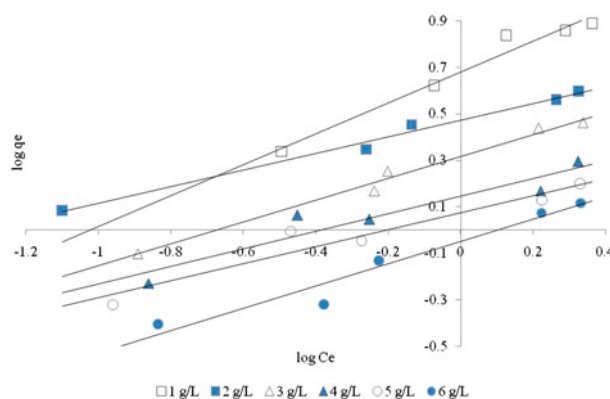
Fig. 6. Freundlich isotherm plots for adsorption of fluoride (concentration: 2.5–20.0 mg/L) on NLP (load: 1.0–6.0 g/L) at 303 K.
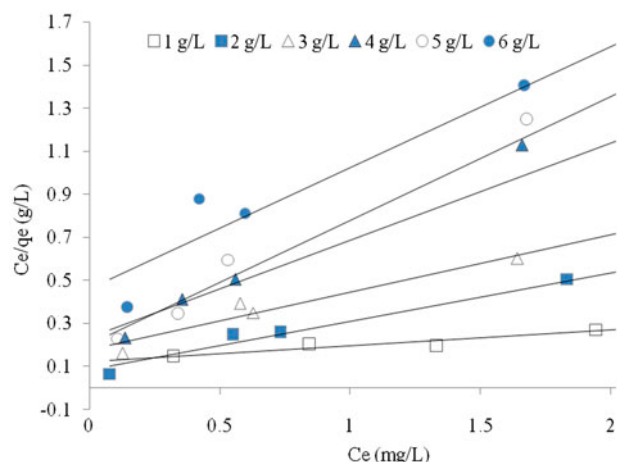
Fig. 7. Langmuir isotherm plots for adsorption of fluoride (concentration: 2.5–20.0 mg/L) on NLP (load: 1.0–6.0 g/L) at 303 K.

on NLP fit both isotherm models reasonably well (Table 3) with good linearity ($R = 0.99$). A better agreement was observed with the Freundlich isotherm ($0 < n < 1$), indicating that the uptake of fluoride on NLP takes place through complex heterogeneous surface processes. Carboxylated cross-linked chitosan beads (CCB) obtained by cross-linking with glutaraldehyde [24], when used as an adsorbent for fluoride, had the maximum adsorption capacity of 11.11 mg/g. The adsorption data fitted both Langmuir and Freundlich isotherms and the adsorption process was spontaneous and endothermic. The defluoridation capacity of protonated cross-linked chitosan beads was also investigated. The maximum adsorption capacity in this case was 7.32 mg/g at 303 K. Meenakshi and Maheshwari also studied the defluoridation capacity of chemically modified chitosan beads by introducing NH_4^+ and COOH groups [25].

A comparison of the Langmuir and Freundlich parameters for fluoride sorption [26–40] on various adsorbents (Table 4) shows that the NLP compares very well with other adsorbents with respect to fluoride adsorption.

3.6. Effects of temperature and thermodynamic study

Adsorption is usually an exothermic process and as the temperature increases, the amount adsorbed at a given concentration decreases in accordance with Le Chatelier's principle. In an independent set of experiments, fluoride adsorption on NLP was studied at three different temperatures from 308 to 318 K and it was found that the extent of adsorption increased with an increase in the temperature (Table 5). Thus, fluoride uptake by NLP was an endothermic process. Equilibrium was approached spontaneously requiring only small external energy input. Similar results have been reported by many other authors [21,24].

The thermodynamic criteria for the adsorption process were evaluated through computation of Gibbs energy (ΔG), enthalpy of adsorption (ΔH) and entropy of adsorption (ΔS) using the following equations:

$$\Delta G = \Delta H - T\Delta S \tag{7}$$

$$\log(q_e/C_e) = -\Delta H/2.303\,RT + \Delta S/2.303\,R \tag{8}$$

where (q_e/C_e) is known as the adsorption affinity equal to the ratio of q_e, the amount adsorbed per unit mass at equilibrium to the equilibrium concentration of the adsorbate, C_e, and R is the universal gas constant (8.314 J/mol/K). The values of ΔH and ΔS were determined from the slope and the intercept of the plots of $\log(q_e/C_e)$ vs. $1/T$. The ΔG values were calculated using Eq. (7). The thermodynamic parameters,

Table 3
Isotherm coefficients for fluoride adsorption on NLP at 303 K (adsorption time: 80 min, fluoride concentration: 2.5, 5.0, 10.0, 15.0 and 20 mg/L, NLP load: 1, 2, 3, 4, 5, 6 g/L)

NLP (g/L)	Langmuir coefficients			Freundlich coefficients		
	R	q_m (mg/g)	R	q_m (mg/g)	R	q_m (mg/g)
1.0	0.97	5.16	5.28	0.98	4.78	0.67
2.0	0.99	3.77	4.08	0.99	2.97	0.36
3.0	0.98	3.27	1.97	0.99	2.08	0.47
4.0	0.97	2.10	2.15	0.98	1.40	0.38
5.0	0.99	1.74	2.83	0.96	1.19	0.37
6.0	0.97	1.78	1.22	0.97	0.89	0.48

Table 4
Langmuir and Freundlich capacities for fluoride adsorption on a few adsorbents

Adsorbent	Langmuir capacity q_{max} (mg/g)	Freundlich capacity K_f (mg/g)	Refs.
ATFSC	22.33	4.53	[26]
BMPSB	2.22	1.40	[27]
Brushite	6.50	2.35	[28]
CBA	7.21	1.66	[29]
CCCB	11.11	0.43	[30]
COIMA	7.22	2.65	[31]
DEW	1.11	1.20	[32]
FCCB	15.39	2.59	[30]
GFH	5.97	3.79	[33]
HCZO	19.40	7.240	[34]
MBC	4.24	0.56	[33]
MCTS	0.22	2.69	[35]
MOCA	2.85	1.10	[36]
PCB	7.32	1.28	[37]
SGCS	8.72	5.886	[38]
Treated alumina	20.41	4.02	[39]
Used tea leaves	23.26	3.16	[39]
ZrIC	4.95	1.24	[40]
NLP	3.77	2.97	This work

Notes: ZrIC Zirconium impregnated cellulose; ATFSC Activated tamarind fruit shell carbon; BMPSB Binary metal oxide-supported beads; CBA Chitosan-based adsorbent; CCCB Carboxylated cross-linked chitosan beads; COIMA Copper oxide-incorporated mesoporous alumina; DEW Disposed earthenware; FCCB Fe(III)-loaded carboxylated chitosan beads; GASS Green algae *Spirogyra* species; MCTS MnO_2-coated tamarind fruit shell; GFH Granular ferric hydroxide; MBC Modified bentonite clay; MOCA Manganese oxide-coated alumina; HCZO Hydrous Ce(IV)–Zr(IV) oxide; SGCS silica gel/chitosan; PCB Protonated chitosan beads.

Table 5
Extent of adsorption of fluoride (2.5 mg/L) at equilibrium (80 min) by different NLP loadings (1.0–6.0 g/L) at three temperatures

Temperature (K)	Extent of adsorption (%)					
	1 g/L	2 g/L	3 g/L	4 g/L	5 g/L	6 g/L
308	27.38	32.11	38.35	36.88	37.24	38.35
313	30.64	45.69	44.95	40.92	41.65	43.85
318	35.78	38.71	51.92	49.72	44.95	52.29

obtained from the plots of log q_e/C_e vs. $1/T$ (Fig. 8), are presented in Table 6.

The enthalpy change, ΔH, decreased slightly from 26.06 to 24.85 kJ/mol as the fluoride concentration increased (2.50–20 mg/L). In the same concentration range, the entropy change, ΔS, varied from −66.92 to 86.47 J/mol/K. Spontaneity of the adsorption process is demonstrated by the decrease in Gibbs energy, ΔG, which varied from −5.75 to −0.99 kJ/mol (fluoride 15.0 mg/L) and from −1.79 to −2.65 kJ/mol (fluoride 20.0 mg/L) in the temperature range of 308–318 K. However, at lower concentrations of fluoride, ΔG had values >0 which still decreased with increasing temperature. It is expected that at lower concentrations

(2.5–10 mg/L), interactions with a positive ΔG occur only if energy is supplied to the system. Similar results were found by Vinitnantharat et al. [8] for the removal of fluoride in aqueous solution by adsorption on acid-activated water treatment sludge.

Negative ΔG values indicate that the equilibrium:

Fluoride (aqueous) + NLP $\rightleftarrows$ Fluoride…NLP

shifts to the forward direction in a spontaneous manner leading to binding of the fluoride ions onto the NLP particles. The randomness at the solid/liquid interface during sorption of fluoride is confirmed by the positive value of ΔS. It is likely that the water
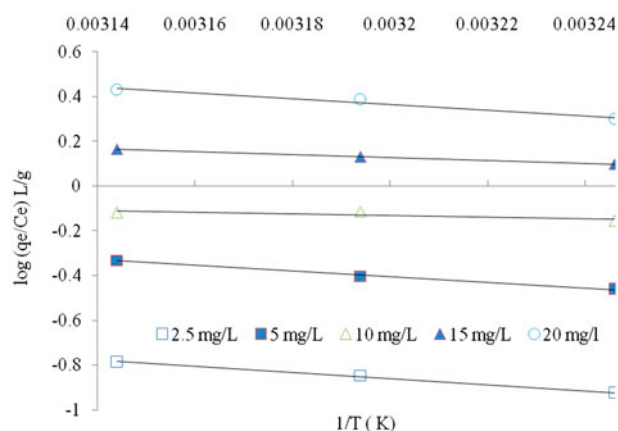
Fig. 8. Plots of $\log(q_e/C_e)$ (L/g) vs. $1/T$ (K) for adsorption of fluoride (concentration: 2.5, 5.0, 10.0, 15.0 and 20.0 mg/L) on NLP (5 g/L) at three different temperatures (308, 313, 318 K).

molecules remaining adsorbed on the NLP surface gain more translational entropy than what is lost by the adsorbed fluoride anions and this increases the randomness of the process [19]. This indicates an increase in the disorder of the system with changes in the hydration of the adsorbing fluoride ions [21]. Similar cases have been reported by Chen et al. [24] showing a positive entropy change (ΔS = 54.557 J/mol/K) for fluoride adsorption on Kanuma mud and hence a good affinity of fluoride ions for the adsorbent surface. Further, the negative Gibbs energy change (ΔG) dictates the feasibility and spontaneity of the adsorption process.

Lv et al. [41] reported an increase in entropy (ΔS 18.4 J/mol/K) and decrease in enthalpy (ΔH −11.67 kJ/mol) as well as Gibbs energy (ΔG −17.12 to 17.76 kJ/mol). Gao et al. [42] have also reported endothermic adsorption (ΔH 37.32 kJ/mol) of fluoride onto synthetic hydroxyapatite.

Similar results, as above, have been reported by Kumar et al. [33] with negative ΔG (−39.22 kJ/mol) and ΔH (7.34 kJ/mol), indicating spontaneous but endothermic nature of the adsorption process between fluoride and granular ferric hydroxide, supported by positive ΔS (158.254 J/mol/K). Jagtap et al. [29] have reported positive ΔH (3.580 kJ/mol) with negative ΔG (22.397–23.640 kJ/mol) and positive ΔS (0.062 J/mol/K). Thakre et al. [27] reported positive ΔH and ΔS of 10.2 kJ/mol and 0.11 kJ/mol/K, respectively, and negative Gibbs energy of −21.975, −23.078 and −24.098 (kJ/mol), respectively, at all temperatures studied.

3.7. Effects of competing ions

Groundwater typically has high concentrations of Na^+, Ca^{2+} and Cl^- in the range of 200–1,200 mg/L and low concentrations of CO_3^{2-}, SO_4^{2-}, Fe^{2+} and NO_3^- in the range of 2–10 mg/L. In this work, the influence of Cl^-, HCO_3^-, SO_4^{2-}, NO_3^- and HPO_4^- on fluoride removal from aqueous solution by adsorption on NLP was investigated. The experimental conditions were: time 80 min (equilibrium time for fluoride adsorption), temperature 303 K (ambient temperature), 25 mL of fluoride solution (concentration 20 mg/L) and 25 ml of the competing ion solution (concentration 20 mg/L) in a binary mixture, taken in 100-ml Kasablanka plastic bottles with different amounts of NLP (1, 2, 3, 4, 5 and 6 g/L). After adsorption, the mixture was filtered and 25 ml of the filtrate was taken for fluoride estimation. Table 7 shows the effects of competing ions on NLP adsorbent capacity for fluoride. A significant influence on fluoride removal was observed in the presence of Cl^-, SO_4^{2-}, HCO_3^- and SO_4^{2-} ions and the defluoridation efficiency decreased from 78.9 to 68.0%. A similar interfering role of the competing ions was reported for defluoridation properties of HFO-doped alginate beads [43].

Table 6
Thermodynamic parameters for adsorption of fluoride on a fixed amount (5.0 g/L) of NLP at constant agitation time of 60 min with different fluoride concentrations (2.5–20 mg/L)

Fluoride (mg/L)	ΔH (kJ/mol)	ΔS (J/mol/K)	ΔG (kJ/mol)		
			308 K	313 K	318 K
2.5	26.06	66.92	5.45	5.11	4.78
5.0	24.29	69.96	2.75	2.40	2.05
10.0	7.13	20.30	0.88	0.78	0.68
15.0	12.42	42.20	−5.75	−0.79	−0.99
20.0	24.85	86.47	−1.79	−2.23	−2.65

Table 7
Influence of competing ions on fluoride adsorption (ratio of fluoride and competing ions 1:1) on NLP at equilibrium time

NLP (g/L)	Percentage adsorption of fluoride in the presence of					
	F^-	Cl^-	NO_3^-	HCO_3^-	HPO_4^-	SO_4^{2-}
1.0	76.9	68.8	71.0	68.9	67.3	68.2
2.0	78.8	70.5	72.6	71.3	67.8	69.1
3.0	78.3	71.1	73.2	73.3	68.6	69.5
4.0	78.9	70.9	72.9	72.5	68.2	69.2
5.0	78.6	70.7	72.7	72.2	68.0	68.9
6.0	78.5	70.1	72.5	72.1	68.5	68.6

3.8. Column adsorption

The column experiment normally aims at determination of the breakthrough point at which effluent concentration becomes almost equal to the initial concentration and the adsorbent bed becomes saturated with the solute.

As the fluoride solution flows downward from the top, the ions adsorb in the column starting from the top and the adsorption zone gradually moves down with more and more solution passing through the column. When the lower edge of the adsorption zone reaches the bottom of the column, adsorption becomes complete and the effluent concentration starts to rise rapidly (Fig. 9). This point gives the breakthrough point, corresponding to which the breakthrough volume, i.e. the volume of the solution (containing a fixed
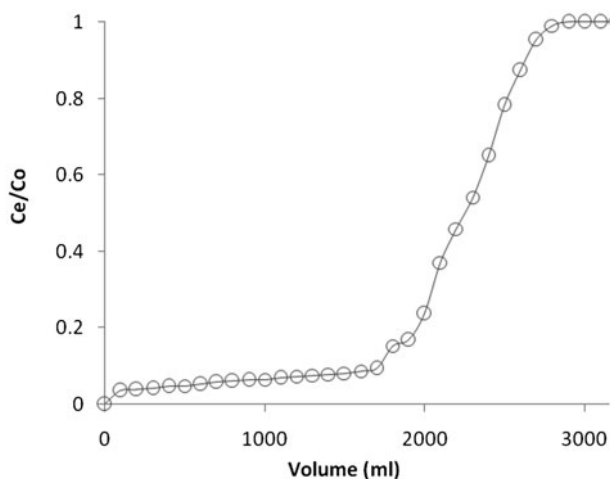
amount of fluoride) which can be safely treated with the column is obtained. The breakthrough volume was 2,800 mL at a fluoride concentration of 20 mg/L, a flow rate of 0.4 mL/min and a NLP bed depth of 1.5 cm.

3.8.1. Effects of bed depth

The effects of biosorbent amount or bed depth on the sorption of fluoride on clay-bound granular sorbent (NLP) were investigated in continuous column mode. The breakthrough curves obtained for fluoride sorption by varying the bed depths from 1.7 to 2.9 cm at a fluoride concentration of 5.0 mg/L and at a constant flow rate of 2.5 mL/min are shown in Fig. 10. The results indicate that with the increase in the bed depth, the breakthrough volume increased because of the rise in the length of the mass transfer zone that ensured a longer contact time between the fluoride ions and the sorbent bed. Such observations for larger fluoride uptake with an increase in the column bed depth have also been reported earlier [29,32].

The fluoride uptake capacity showed an increasing trend (3.17–3.40 mg/g for 90% breakthrough and 1.83–2.00 mg/g for 50% breakthrough) with increasing bed depth from 1.7 to 2.9 cm (Table 8). Although, the sorption capacities at 90% and 50% breakthrough points for the clay-bound NLP showed an increasing tend with increasing bed depth, the breakthrough capacities did not show much variation at different bed depths (Table 8). This trend is expected because the uptake capacity usually depends on the amount of sorbent available for sorption. Naturally, the availability of more adsorbent at higher bed depths offers more surface area and binding sites for sorption resulting in

Fig. 9. Breakthrough curve for column adsorption of fluoride (20 mg/L) (clay-bound NLP granules, bed height: 1.5 cm, flow rate: 0.4 mL/min).
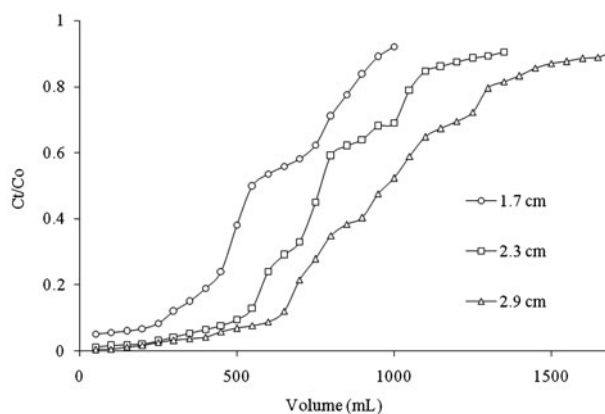
Fig. 10. Effects of bed depth (clay-bound NLP granules) on sorption of fluoride on NLP at 303 K (flow rate: 2.5 mL/min, feed concentration: 5.0 mg/L).

Table 8
Column adsorption capacities of clay-bound NLP at 50 and 90% breakthrough points for a fixed fluoride concentration of 5.0 mg/L at 303 K. (BV = Breakthrough volume; Ad. Cap = Adsorption capacity)

Sorbents	Flow rate (mL/min)	Bed depth (cm)	90% breakthrough			50% breakthrough		
			BV (mL)	Time (min)	Ad.Cap (mg/g)	BV (mL)	Time (min)	Ad. Cap (mg/g)
NLP	2.5	1.7	960	400.0	3.17	550	220.0	1.83
		2.3	1,400	550.0	3.38	750	300.0	1.88
		2.9	1,700	680.0	3.40	1,000	400.0	2.00

enlarged mass transfer [29,44]. Similar results for the effects of bed depth on the adsorption of fluoride were reported for a bottom ash bed [39].

3.8.2. Effects of flow rate

The breakthrough curves at three different flow rates obtained by plotting the ratio of effluent to influent concentrations (C_t/C_o) against the effluent volume (mL) for the clay-bound biosorbent at a constant bed depth of 2.3 cm and a constant fluoride concentration of 5 mg/L are shown in Fig. 11.

The decrease in sorption capacity with an increase in the flow rates is due to insufficient contact time between fluoride ions with the sorbent bed and the diffusion limitations of the solute into the pores of the sorbent at higher flow rates. However, at lower flow rate, interactions between the adsorbent and fluoride ions had ample time, resulting in a higher fluoride sorption capacity [41,44]. Similar results were reported in the literature for the effects of flow rates on the sorption of fluoride in fixed-bed system using activated alumina [45] and sugarcane charcoal [46].
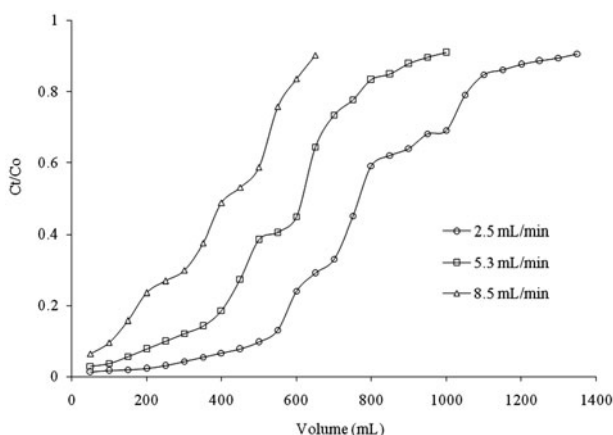
Fig. 11. Effects of flow rate on sorption of fluoride on clay-bound NLP at 303 K (bed depth: 2.3 cm, fluoride concentration: 5.0 mg/L).

It was observed that the breakthrough curves had very similar features: steep at higher flow rates indicating quick saturation of the sorbent bed. This might be due to a faster movement of the adsorption zone at higher flow rates. Further, with an increase in the flow rate, all the three parameters, i.e. breakthrough time, breakthrough volume and breakthrough capacity, at 50 and 90% breakthrough points decreased (Table 7). These results indicate that the column performs well at the lowest flow rate. The fluoride adsorption capacities (mg/g) of the clay-bound biosorbent at 50 and 90% breakthrough points at three different flow rates (fluoride concentration 5.0 mg/L, bed depth 2.3 cm, 303 K) are presented in Table 8.

Sulaiman et al. [45] had reported that both breakthrough times and fluoride sorption capacity of alumina cement granules at different bed depths of 5, 10 and 15 cm for a particular flow rate of 8 mL/min increased with a corresponding increase in bed depths. They had reported that fluoride uptake capacity of the alumina cement granules increased from 0.317 to 0.402 mg/g as the bed depths increased from 5 to 15 cm for a constant flow rate of 8 mL/min. Viswanathan et al. [37] have also made similar observations for fluoride sorption on activated tamarind fruit fhell (ATFS) and MnO_2-coated tamarind fruit shell (MTFS) columns. Similar results for the removal of fluoride in a fixed-bed system have been reported for the effects of bed depths using manganese oxide-coated alumina, Kunuma mud and sugarcane charcoal [46].

3.8.3. Effects of fluoride concentration

The change in the initial fluoride concentration has a significant effect on the breakthrough curves. The clay-bound biosorbent (NLP) was investigated in column mode at three initial fluoride concentrations of 5.0, 10.0 and 15.0 mg/L with a constant bed depth of 2.3 cm and a fixed flow rate of 2.5 mL/min. The breakthrough curves obtained by changing the initial fluoride concentration from 5 to 15 mg/L are given in Fig. 12.

The breakthrough volume was found to depend on the flow rate and a slower flow rate yielded a larger breakthrough volume. If the curve rises steeply after reaching the breakthrough point, it is indicative of a shorter adsorption zone, which is completely saturated with the adsorbate. On the other hand, a less sharp curve after reaching the breakthrough point indicates a longer adsorption zone. In designing a column, the length of the adsorption zone represents the minimum bed depth required to produce a low-effluent fluoride concentration.

Similar results regarding the effects of initial fluoride concentration have been reported in a fixed-bed system using granular red mud and Kunuma mud [46]. Lavecchia et al. [47] reported that fluoride adsorption capacity of high-alumina content bauxite increased from 1.08 to 1.79 mg/g as the initial fluoride concentration increased from 5.0 to 50 mg/L for a constant flow rate of 0.50 cm^3/min. Mondol et al. [46] had recently reported that fluoride adsorption capacity of sugarcane charcoal increased from 2.34 to 12.6 mg/g as the initial fluoride concentration was increased from 3.0 to 10.0 mg/L for a constant bed depth of 16.7 cm at the flow rate of 4.34 mL/min. They had also reported that as the fluoride concentration increased from 3.0 to 10.0 mg/L, the breakthrough time decreased from 200 to 50 min for a constant bed depth and flow rate of 16.7 cm and 4.34 mL/min, respectively.

3.8.4. Interpretation of column study data with Bohart–Adams model

The dynamic behaviour of a solute in a fixed bed under defined operating conditions is difficult to predict because the process does not occur at a steady state, while the influent still passes through the bed. Uneven flow pattern throughout the column usually results in an incomplete exhaustion of the bed. Therefore, a successful design of a column adsorption process requires a description of the dynamic behaviour of adsorbate in a fixed bed. A simplified form of the Bohart–Adams Model [47] is:
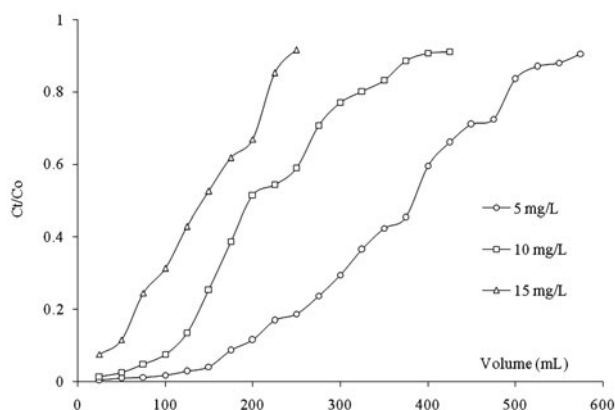
$$t_b = aD + b \qquad (9)$$

where $a = N_o/(C_o)$ and $b = -1/(C_o k)\ln(C_o/C_b - 1)$.

The two coefficients, a and b, in the BDST model are obtained from the slope and the intercept is obtained from the plots of time against bed depth (iso-removal lines). The BDST equation describes how the mass transfer zone progresses through a single fixed bed of adsorbent. For getting accurate results, the required condition is that the MTZ should move through the column at a constant rate and so a constant pattern of MTZ, a constant feed concentration and a constant feed flow rate are required. In the present work, the BDST model is used to describe and predict the dynamic behaviour of the clay-bound biosorbent beds in column performance. Table 9 shows the BDST model parameters for the column sorption of fluoride on NLP.

In the present study, the BDST plots (Fig. 13) for the clay-bound biosorbent at 20, 40, 60 and 80% breakthrough concentrations are linear. The mean correlation coefficient (r) of 0.99, 0.98, 0.93 and 0.99 for 20, 40, 60 and 80% breakthrough indicated the validity of the BDST model for fluoride–clay-bound biosorbent sorption system. The BDST model parameters, viz. N_o (the adsorption capacity) and k (adsorption rate coefficient) obtained from the slopes and intercepts of the isoremoval lines, are presented in Table 8. It is observed that the sorption capacity (N_o) increases from 0.78 to 1.25 g/L as the breakthrough value rises from 20 to 80%, indicating that the column becomes saturated with the fluoride ions gradually and the number of available adsorption sites decreases with time [27].

The rate coefficient, k, of the BDST model increased from −399.2 to 131.3 L/g/h as the breakthrough increased from 20 to 80% for fluoride adsorption on a clay-bound NLP column. This indicates a positive correlation between the rate coefficient, k, and the breakthrough values and an increasing capacity of the column for the removal of fluoride from the solution.

3.9. Desorption and regeneration study

Desorption and regeneration study is very essential from economical and practical points of view. In the

Fig. 12. Effects of fluoride concentration on its adsorption on clay-bound NLP (bed depth: 2.3 cm, flow rate: 2.5 mL/min) at 303 K.

Table 9
BDST model parameters for column sorption of fluoride on clay-bound NLP

Breakthrough point (%)	Slope	Intercept	Adsorption capacity, N_o (g/L)	k (L/g/h)	Regression coefficient (r)
20	83.3	41.7	0.78	−399.2	0.99
40	100.0	43.3	0.94	−112.3	0.93
60	116.7	71.7	1.10	67.1	0.97
80	133.3	126.7	1.25	131.3	0.99
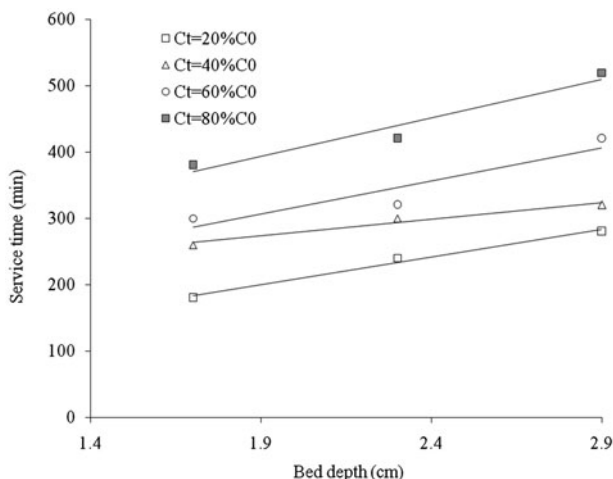
Fig. 13. Iso-removal lines for sorption of fluoride on clay-bound NLP at 303 K (flow rate: 2.5 mL/min, fluoride concentration: 5.0 mg/L).

Fig. 14. Desorption of fluoride from fluoride-loaded clay-bound NLP at 303 K with aqueous 0.1 N NaOH (bed depth: 2.3 cm, flow rate: 2.2 mL/min).

present work, the column with clay-bound NLP bed depth of 2.3 cm was selected for desorption study. The column was first saturated with fluoride ions by passing a fluoride solution of concentration 5.0 mg/L and then the adsorbed fluoride ions were eluted from the fluoride-loaded sorbent bed using 0.1 N NaOH (pH 10.0) as the eluent at a constant flow rate. The concentration of fluoride in the eluate in each case was monitored with a cumulative volume. The desorption flow rate (2.2 mL/min) was slightly less than the sorption flow rate (2.5 mL/min) such that the regenerate was high in fluoride concentration and less in volume, which is economical for the recovery of fluoride and could help in easy handling [48]. Aqueous NaOH was selected as the eluent because it was reported to be efficient in removing fluoride from adsorbed beds in various works [24,49]. Aqueous NaOH was also used as the eluent to desorb the pre-adsorbed fluoride from fluoride-loaded chitin and chitin-based biocomposite [29]. During desorption, NaOH increases the solution pH inside the packed columns and allows the adsorbed fluoride ions to

desorb as NaF [29]. The volume required to desorb the pre-adsorbed fluoride from chitin and chitin-based biocomposite beds was 93.2 and 176.4 mL, respectively.

In the present work, it was observed that dilute NaOH (0.1 N) was efficient in removing fluoride from the clay-bound biosorbent and almost 100% fluoride could be recovered from the fluoride-loaded biosorbent (Fig. 14). It is thus likely that the fluoride ions were held to the sorbent surface mainly through ion-exchange type of interactions. Complete desorption of fluoride from a column of bed height 2.5 cm was possible in 350.0 min with 800 mL of 0.1 N NaOH.

4. Conclusion

It can be concluded that the adsorbent NLP prepared from *A. indica* leaf powder has shown excellent adsorption capacity for fluoride. The adsorptive removal of fluoride increased with increasing pH and maximum fluoride removal occurred at a pH of 6.4. Besides, the fluoride removal increased with increasing contact time, temperature and adsorbent amount. The presence of chloride ions reduced the rate of diffusion of the fluoride ions to the surface of the adsorbent and hence adversely affected fluoride

removal. It was further observed that the equilibrium behaviour can be well predicted by application of the Langmuir adsorption isotherm.

References

[1] World Health Organization, Guidelines for Drinking Water Quality: Incorporating First Addendum Recommendations, vol. 1, third ed., World Health Organization, Geneva, Switzerland, 2006.

[2] S. Ayoob, A.K. Gupta, Fluoride in drinking water: A review on the status and stress effects, Crit. Rev. Environ. Sci. Technol. 36 (2006) 433–487.

[3] S.V. Ramanaiah, S. Venkata Mohan, B. Rajkumar, P.N. Sarma, Monitoring of fluoride concentration in ground water of Prakasham district in India: Correlation with physicochemical parameters, J. Environ. Sci. Eng. 48 (2006) 129–134.

[4] K. Zhang, S. Wu, X. Wang, J. He, B. Sun, Y. Jia, T. Luo, F. Meng, Z. Jin, D. Lin, W. Shen, L. Kong, J. Liu, Wide pH range for fluoride removal from water by MHS-MgO/MgCO$_3$ adsorbent: Kinetic, thermodynamic and mechanism studies, J. Colloid Interface Sci. 446 (2015) 194–202.

[5] G.M. Gadd, Biosorption: Critical review of scientific rationale, environmental importance and significance for pollution treatment, J. Chem. Technol. Biotechnol. 84 (2009) 13–20.

[6] W.S. Wan Ngah, M.A.K.M. Hanafiah, Removal of heavy metal ions from wastewater by chemically modified plant wastes as adsorbents: A review, Bioresour. Technol. 99 (2008) 3935–3948.

[7] S. Venkatamohan, S.V. Ramanaiah, B. Rajkumar, P.N. Sarma, Removal of fluoride from aqueous phase by biosorption onto algal biosorbent *Spirogyra* Sp. I02: Sorption mechanism elucidation, J. Hazard. Mater. 141 (2007) 465.

[8] S. Vinitnantharat, S. Kositchaiyong, S. Chiarakorn, Removal of fluoride in aqueous solution by adsorption on acid activated water treatment sludge, Appl. Surf. Sci. 256 (2010) 5458.

[9] A. Sharma, K.G. Bhattacharyya, *Azadirachta indica* (Neem) leaf powder as a biosorbent for removal of Cd (II) from aqueous medium, J. Hazard. Mater. 125 (2005) 102.

[10] J. Sarma, A. Sarma, K.G. Bhattacharyya, Biosorption of commercial dyes on *Azadirachta indica* leaf powder: A case study with a basic dye, rhodamine B, Ind. Eng. Chem. Res. 47 (2008) 5433.

[11] APHA, Standard Methods for Examination of Water and Wastewater, twentieth ed., American Public Health Association, Washington, DC, 1998.

[12] M. Mohapatra, T. Padhi, S. Anand, B.K. Mishra, CTAB mediated Mg-doped nano Fe$_2$O$_3$: Synthesis, characterization, and fluoride adsorption behaviour, Desalin. Water Treat. 50 (2013) 376–386.

[13] S.K. Swain, T. Patnaik, P.C. Patnaik, U. Jha, R.K. Dey, Development of new alginate entrapped Fe(III)–Zr(IV) binary mixed oxide for removal of fluoride from water bodies, Chem. Eng. J. 215–216 (2013) 763.

[14] S. Venkata Mohan, J. Karthikeyan, Removal of lignin and tannin aqueous solution by adsorption onto activated charcoal, Environ. Pollut. 97 (1997) 183–197.

[15] T. Ilhami, B. Gulay, Y. Emine, B. Gokben, Equilibrium and kinetic studies on biosorption of Hg(II), Cd(II) and Pb(II) ions onto micro algae *Chlamydomonas reinhardtii*, J. Environ. Manage. 77 (2005) 85.

[16] S. Venkata Mohan, Y. Vijaya Bhaskar, J. Karthikeyan, Biological decolorization of simulated azo dye in aqueous phase by algae *Spirogyra* species, Int. J. Environ. Pollut. 21 (2003) 211.

[17] Y. Tian, M. Wu, R. Liu, D. Wang, X. Lin, W. Liu, L. Ma, Y. Li, Modified native cellulose fibers—A novel efficient adsorbent for both fluoride and arsenic, J. Hazard. Mater. 185 (2011) 93.

[18] N. Viswanathan, S. Meenakshi, Development of chitosan supported zirconium(IV) tungstophosphate composite for fluoride removal, J. Hazard. Mater. 176 (2010) 459.

[19] W.J. Weber, J.C. Morris, Kinetics of adsorption on carbon from solution, J. Sanitary Eng. Div. Proceed. Am. Soc. Civil Eng. 89 (1963) 31.

[20] S. Dhiman, J. Rajib, S. Mitali, Taguchi design and equilibrium modeling for fluoride adsorption on cerium loaded cellulose nanocomposite bead, Carbohydr. Polym. 111 (2014) 813.

[21] W. Dongjin, L. Yongde, X. Shuhu, C. Jing, Z. Jian, Uptake fluoride from water by caclined Mg-Al-CO3 hydrotalcite: Mg/Al ratio effect on its structure, electrical affinity and adsorptive Property, Colloids Surf. A: Physicochem. Eng. Aspects 469 (2015) 307.

[22] H.M.F. Freundlich, Über die Adsorption in Lösungen (About the adsorption in solutions), Z. Phys. Chem 57A (1906) 385–470.

[23] I. Langmuir, The constitution and fundamental properties of solids and liquids, J. Am. Chem. Soc. 38 (1916) 2221.

[24] N. Chen, Z. Zhang, C. Feng, D. Zhu, Y. Yang, N. Sugiura, Preparation and characterization of porous granular ceramic containing dispersed aluminum and iron oxides as adsorbents for fluoride removal from aqueous solution, J. Hazard. Mater. 186 (2011) 863.

[25] R. Meenakshi, R.C. Maheshwari, Fluoride in drinking water and its removal, J. Hazard. Mater. 137 (2006) 456.

[26] V. Sivasankar, S. Rajkumar, S. Murugesh, A. Darchen, Influence of shaking or stirring dynamic methods in the defluoridation behavior of activated tamarind fruit shell carbon, Chem. Eng. J. 197 (2012) 162.

[27] D. Thakre, S. Jagtap, N. Sakhare, N. Labhsetwar, S. Meshram, S. Rayalu, Chitosan based mesoporous Ti–Al binary metal oxide supported beads for defluoridation of water, Chem. Eng. J. 158 (2010) 315.

[28] M. Mourabet, H. El Boujaady, A. El Rhilassi, H. Ramdane, M. Bennani-Ziatni, R. El Hamri, A. Taitai,

Defluoridation of water using Brushite: Equilibrium, kinetic and thermodynamic studies, Desalination 278 (2011) 1.

[29] S. Jagtap, M.K.N. Yenkie, N. Labhsetwar, S. Rayalu, Defluoridation of drinking water using chitosan based mesoporous alumina, Microporous Mesoporous Mater. 142 (2011) 454.

[30] N. Viswanathan, S. Meenakshi, Selective sorption of fluoride using Fe(III) loaded carboxylated chitosan beads, J. Fluorine Chem. 129 (2008) 503.

[31] A. Bansiwal, P. Pillewan, R.B. Biniwale, S.S. Rayalu, Copper oxide incorporated mesoporous alumina for defluoridation of drinking water, Microporous Mesoporous Mater. 129 (2010) 54.

[32] V. Sivasankar, T. Ramachandramoorthy, A. Darchen, Manganese dioxide improves the efficiency of earthenware in fluoride removal from drinking water, Desalination 272 (2011) 179.

[33] E. Kumar, A. Bhatnagar, M. Ji, W. Jung, S.H. Lee, S.J. Kim, G. Lee, H. Song, J.Y. Choi, J.S. Yang, B.H. Jeon, Defluoridation from aqueous solutions by granular ferric hydroxide (GFH), Water Res. 43 (2009) 490.

[34] A. Ghosh, S. Chakrabarti, K. Biswas, U.C. Ghosh, Agglomerated nanoparticles of hydrous Ce(IV) + Zr (IV) mixed oxide: Preparation, characterization and physicochemical aspects on fluoride adsorption, Appl. Surf. Sci. 307 (2014) 665.

[35] V. Sivasankar, T. Ramachandramoorthy, A. Chandramohan, Fluoride removal from water using activated and MnO_2-coated Tamarind Fruit (*Tamarindus indica*) shell: Batch and column studies, J. Hazard. Mater. 177 (2010) 719.

[36] S.M. Maliyekkal, A.K. Sharma, L. Philip, Manganese-oxide-coated alumina: A promising sorbent for defluoridation of water, Water Res. 40 (2006) 3497.

[37] N. Viswanathan, C.S. Sundaram, S. Meenakshi, Removal of fluoride from aqueous solution using protonated chitosan beads, J. Hazard. Mater. 161 (2009) 423.

[38] S.M. Prabhu, S. Meenakshi, Enriched fluoride sorption using chitosan supported mixed metal oxides beads: Synthesis, characterization and mechanism, J. Water Process Eng. 2 (2014) 96.

[39] A.D. Dwivedi, S.P. Dubey, K. Gopal, V.K. Tandon, A comparative investigation for strengthening the adsorptive phenomenon by activated natural minerals and plant waste-carbon for defluoridation in water milieu, Desalination 263 (2010) 189.

[40] M. Barathi, A. Santhana Krishna Kumar, N. Rajesh, A novel ultrasonication method in the preparation of zirconium impregnated cellulose for effective fluoride adsorption, Ultrason. Sonochem. 21 (2014) 1090.

[41] L. Lv, J. He, M. Wei, D.G. Evans, Z. Zhou, Treatment of high fluoride concentration water by $MgAl-CO_3$ layered double hydroxides: Kinetic and equilibrium studies, Water Res. 41 (2007) 1534.

[42] S. Gao, J. Cui, Z. Wei, Study on the fluoride adsorption of various apatite materials in aqueous solution, J. Fluorine Chem. 130 (2009) 1035.

[43] M.G. Sujana, A. Mishra, B.C. Acharya, Hydrous ferric oxide doped alginate beads for fluoride removal: Adsorption kinetics and equilibrium studies, Appl. Surf. Sci. 270 (2013) 767.

[44] M. Sarkar, A. Banerjee, P.P. Pramanick, A.R. Sarkar, Design and operation of fixed bed laterite column for the removal of fluoride from water, Chem. Eng. J. 131 (2007) 329.

[45] A. Sulaiman, A.K. Gupta, A.B. Basheer, A fixed bed sorption system for defluoridation of ground water, J. Urban Environ. Eng. 3 (2009) 17.

[46] N.K. Mondol, R. Bhaumik, P. Roy, B. Das, J.K. Datta, Investigation on fixed bed column performance of fluoride adsorption by sugarcane charcoal, J. Environ. Biol. 34 (2013) 1059.

[47] R. Lavecchia, F. Medici, L. Piga, G. Rinaldi, A. Zuorro, Fluoride removal from water by adsorption on a high alumina content bauxite, Chem. Eng. Trans. 26 (2012) 225.

[48] U. Kumar, M. Bandyopadhyay, Fixed bed column study for Cd(II) removal from wastewater using treated rice husk, J. Hazard. Mater. 129 (2006) 253.

[49] W. Ma, F. Ya, R. Wang, Y.Q. Zhao, Fluoride removal from drinking water by adsorption using bone char as a biosorbent, Int. J. Environ. Technol. Manage. 9 (2008) 59.